Acta Crystallographica Section B
**Structural Science**
ISSN 0108-7681

# Structure of strontium barium niobate $Sr_xBa_{1-x}Nb_2O_6$ (SBN) in the composition range $0.32 \leq x \leq 0.82$

**Sergey Podlozhenov,[a] Heribert A. Graetsch,[b] Julius Schneider,[c] Michael Ulex,[a] Manfred Wöhlecke[a] and Klaus Betzler[a]***

[a]Fachbereich Physik, Universität Osnabrück, D-49069 Osnabrück, Germany, [b]Ruhr-Universität Bochum, D-44801 Bochum, Germany, and [c]Ludwig-Maximilians-Universität, D-80333 München, Germany

Correspondence e-mail: klaus.betzler@uos.de

Received 21 March 2006
Accepted 22 September 2006

The structure of strontium barium niobate crystals $Sr_xBa_{1-x}Nb_2O_6$ is comprehensively studied in the whole range of the tetragonal tungsten bronze phase ($x$ = 0.32–0.82) using both powder and single-crystal X-ray diffraction measurements. Unit-cell parameters, density, site-occupancy factors and interionic distances show an explicit composition dependence which can be consistently explained using simple model calculations. The temperature dependence of the unit-cell parameters exhibits a remarkable anisotropy in a broad temperature region below the phase transition temperature. This proves that the electrostrictive contribution to the thermal expansion plays an important role in strontium barium niobate.

## 1. Introduction

Strontium barium niobate, $Sr_xBa_{1-x}Nb_2O_6$ (SBN), is an extensively studied ferroelectric material for electrooptic and photorefractive applications owing to its high electrooptic ($r_{33}$ = 420 pm $V^{-1}$ for $x$ = 0.61) and piezoelectric coefficients (Neurgaonkar *et al.*, 1984). Utilizing the high four-wave coupling coefficient $\Gamma$ in Ce-doped SBN, holographic applications of doped SBN (Volk *et al.*, 1997) were also investigated. Most investigations were restricted to the congruently melting composition with $x$ = 0.61, because for this composition crystals of high optical quality are available. The motivation to study SBN crystals with other strontium concentrations is the strong compositional dependence of the phase transition temperature. It changes from 503 K for $x$ = 0.32 to *ca* 283 K for $x$ = 0.82 (David *et al.*, 2004). Taking advantage of this dependence, the electrooptic coefficients for room temperature can be optimized using appropriate Sr concentrations ($r_{33}$ = 1400 for $x$ = 0.75; Neurgaonkar *et al.*, 1984).

SBN belongs to the group of *relaxor* ferroelectrics. A typical phenomenon for this class is a broadened phase transition which is probably caused by the wide variation of the non-equivalent crystallographic positions in its structure. A first structural characterization was made in 1969 (Jamieson *et al.*, 1968) for the composition $x$ = 0.75. The ferroelectric relaxor SBN belongs to the structure type of tetragonal tungsten bronze (TTB) with the space group $P4bm$ at room temperature (see Fig. 1). Sr and Ba occupy the $A1$ and $A2$ positions; while the smaller 12-fold coordinated $A1$ site is occupied only by Sr, both Sr and Ba are found in the larger 15-fold coordinated $A2$ site. This cation distribution was recently confirmed for SBN crystals with $x$ = 0.61 (Chernaya *et al.*, 1997) and 0.75 (Chernaya *et al.*, 2000).

The compositional range of the ferroelectric TTB phase has usually been defined as $x$ = 0.25–0.75. The existence range of

tetragonal SBN was recently corrected to be $x$ = 0.32–0.82 (Ulex *et al.*, 2004). The aim of this work is a structure determination for the whole compositional range of SBN by means of X-ray diffraction measurements for both single-crystal and powder samples, with special attention on the cation distribution and the parameters of the Nb coordination polyhedron in the unit cell.

## 2. Experimental

### 2.1. Crystals

Single crystals of SBN ($x$ = 0.32–0.82) were grown by the Czochralski technique using resistance heating. The detailed description of growth procedures can be found elsewhere (Ulex *et al.*, 2004). The crystals were grown along the [001] direction; they exhibit a slight yellow colouration and show the form of prisms with 16 natural facets. The crystal diameter is between 5 and 7 mm. For the single-crystal X-ray measurements, as-grown (unpoled) single crystals were ground in an agate mortar followed by grinding in a ball mill. These operations produced single-crystalline spherical particles with diameters between 50 and 100$\mu$m. The samples for the powder X-ray diffractometry were also produced by grinding grown crystals.

### 2.2. X-ray diffraction measurements

X-ray powder diffraction measurements were performed on crystal powder samples consisting of 40 mg SBN and 12 mg F-phlogopite as standard, using Cu $K\alpha$ radiation. The single-crystal X-ray diffraction measurements were carried out on a four-circle kappa diffractometer (Xcalibur from Oxford Diffraction) equipped with a Sapphire2 CCD area detector. Graphite-monochromatized Mo $K\alpha$ radiation was used. The sample-to-detector distance was 44.4 mm. With one and four scans, 93.2% of reciprocal space was covered which corresponds to 100% completeness under Laue group 4/$m$ mm at a resolution of 0.8 Å. Data reduction and numerical absorption correction were carried out with the program *CrysAlisRED* (Oxford Diffraction, 2002). The crystal structure was refined with the program *SHELXL*97 (Sheldrick, 1997).

All measurements (except those for the temperature dependence of the unit-cell parameters) were carried out at room temperature.

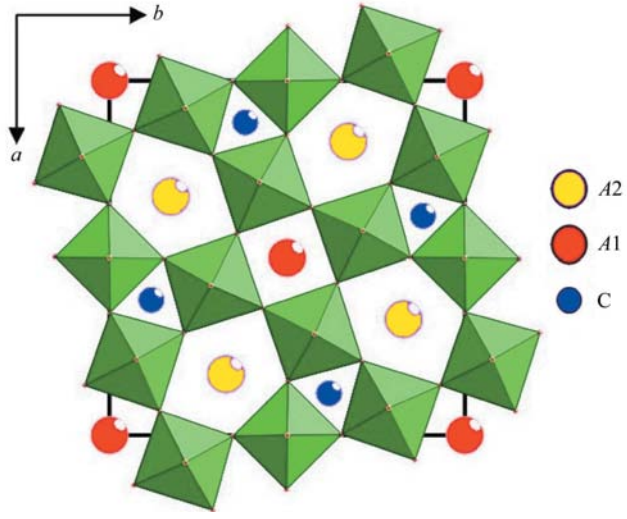


**Figure 1**
Crystal structure of the tetragonal tungsten bronze.

## 3. Results and discussion

### 3.1. Unit-cell parameters

Powder X-ray measurements were performed throughout the compositional range $x$(Sr) from 0.32 to 0.82 with composition steps of *ca* 0.03. From these measurements, the unit-cell

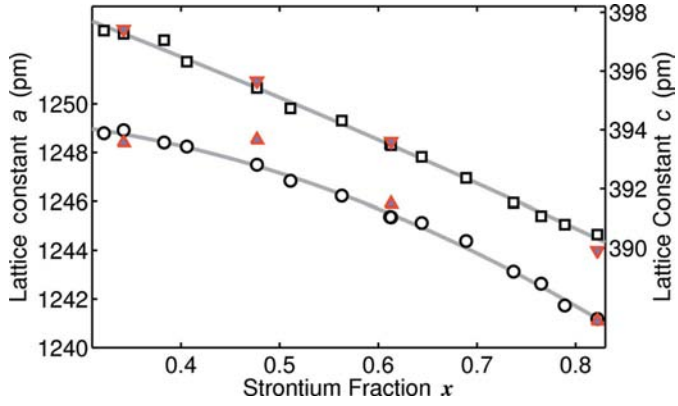


**Figure 2**
Unit-cell parameters of strontium barium niobate $Sr_xBa_{1-x}Nb_2O_6$ as a function of the strontium content $x$ derived from powder (circles and squares) and single-crystal (filled triangles) X-ray measurements. Lines denote fits to the powder data.

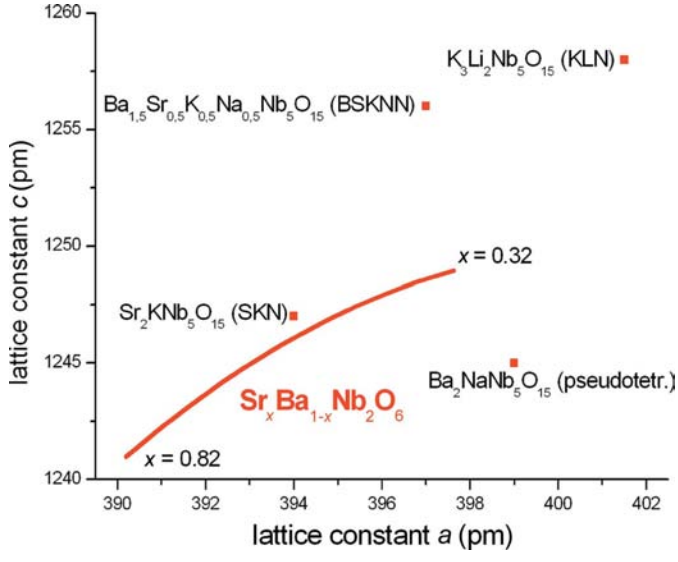


**Figure 3**
SBN unit-cell parameters compared with other ferroelectrics from the TTB family (after Neurgaonkar & Cory, 1986).

parameters $a$ and $c$ could be derived with an accuracy of approximately $3 \times 10^{-5}$.

The $a$ parameter lies between 1248.5 and 1241.1 pm and the $c$ parameter varies from 397.4 to 389.9 pm. Both $a$ and $c$ unit-cell parameters decrease with increasing Sr concentration. The dependence of the unit-cell parameters on the Sr concentration is shown in Fig. 2. The unit-cell parameters for the composition $x = 0.61$ are in good agreement with previously reported data (Chernaya *et al.*, 1997). For comparison, the unit-cell parameters resulting from the single-crystal measurements (see below) are also plotted.

The composition dependence of the unit-cell parameters can be described using second-order polynomial fits to the powder data

$$a = 1249.2 + 4.75x - 17.6x^2 \quad (1)$$

$$c = 401.55 - 11.70x - 2.41x^2 \quad (2)$$

plotted as lines in Fig. 2. A quadratic term is included in both (1) and (2) to account for the slight deviations from Vegard's rule visible in the data. From Vegard's rule, a strictly linear dependence would be expected.

The overall variation of the unit-cell volume is approximately 3%. This can be fully ascribed to the variation of the effective average radii $r_{\rm eff}$ of the cations occupying the $A1$ and $A2$ sites ($r_{\rm eff}$ = 142–134 pm for $r_{\rm Ba}$ = 147 pm and $r_{\rm Sr}$ = 131 pm (Shannon & Prewitt, 1969, 1970), if one takes into account that approximately 15% of the unit-cell volume belongs to the $A1$ and $A2$ sites.

In Fig. 3 the measured unit-cell values are compared with the data for other ferroelectrics with the TTB structure. The Sr-rich compositions of SBN show rather small unit-cell parameters. This could be one of the reasons for the high values of the spontaneous polarization $P_{\rm s}$ and in turn the electrooptic coefficient $r_{ij}$ in SBN.

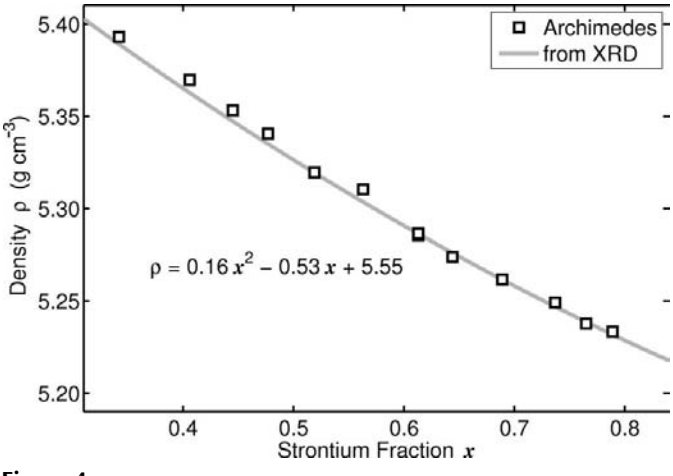


**Figure 4**
Density of SBN as a function of the Sr content. Squares denote measured data (Archimedes principle); the line shows the X-ray density calculated using the unit-cell parameters.

### 3.2. Density

The density of the crystals was measured by hydrostatic technique on SBN samples with a typical volume of some cubic centimeters using distilled water as the immersion liquid. Thus, a good accuracy was achieved. The results are plotted in Fig. 4 together with the calculated X-ray density. For the calculation, the composition-dependent unit-cell parameters as given in (1) and (2) are used. A second-order polynomial fit to the X-ray density yields

$$\rho = 0.16x^2 - 0.53x + 5.55. \quad (3)$$

Again the quadratic term is included to account for deviations from Vegard's rule.

### 3.3. Site-occupancy factors

Single-crystal X-ray diffraction measurements were performed on $Sr_xBa_{1-x}Nb_2O_6$ crystals with $x$ equal to 0.342, 0.477, 0.613 and 0.822. For all these compositions the structure refinement led to the tetragonal structure type with the space group $P4bm$.

The site-occupancy factors (s.o.f.) for the cation sites $A1$ and $A2$, derived from the measurement, are shown in Fig. 5. Site-occupancy factors are defined as

$$\text{s.o.f.}_i = M_i N/Z, \quad (4)$$

where $M_i$ is the number of atoms per formula unit on site $i$, $N$ the number of formula units per unit cell and $Z$ the number of symmetry-equivalent sites in the unit cell. For SBN, $N = 5$, $Z = 8$, and the sum of the $M_i$ for the $A1$ and $A2$ sites is 1. The 12-fold coordinated $A1$ sites are occupied by Sr cations only, the site-occupancy factor s.o.f.(Sr—$A1$) depends only slightly on the composition and varies between 0.16 and 0.18 corresponding to a relative occupancy between 66 and 72%. The 15-fold coordinated $A2$ sites are occupied by both Sr and Ba cations with an approximately linear composition dependence

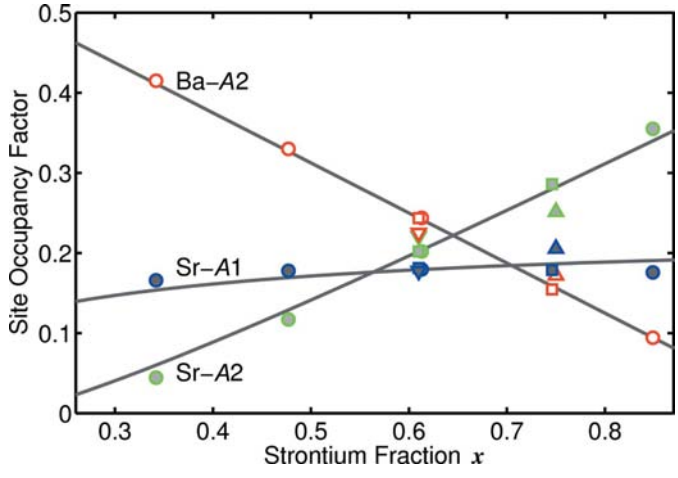


**Figure 5**
Site-occupancy factors for $A1$ and $A2$ sites in SBN. Dots indicate measured data: ○ – this work; △ – Jamieson *et al.* (1968); □ – Chernaya *et al.* (1997); ▽ – Woike *et al.* (2003). The lines represent the results of a model calculation (see text).

**Table 1**
Results of the X-ray diffraction measurements on $Sr_xBa_{1-x}Nb_2O_6$ single crystals of different strontium fraction $x$.

| Crystal | | SBN-34 | SBN-48 | SBN-61 | SBN-82 |
|---|---|---|---|---|---|
| Strontium fraction | $x$ | 0.342 | 0.477 | 0.613 | 0.822 |
| Cell parameters | $a$ (pm) | 1248.40 (4) | 1248.52 (6) | 1245.9 (1) | 1241.1 (5) |
| | $c$ (pm) | 397.42 (3) | 395.66 (5) | 393.6 (1) | 389.9 (2) |
| Site occupancy | Sr—$A1$ | 0.1659 (3) | 0.1777 (3) | 0.1796 (3) | 0.1758 (5) |
| | Ba—$A2$ | 0.4150 (4) | 0.3300 (4) | 0.2438 (4) | 0.0942 (6) |
| | Sr—$A2$ | 0.0444 (4) | 0.1170 (4) | 0.2019 (4) | 0.3550 (6) |
| Nb—O distance | Nb1 (pm) | 197.10 | 197.01 | 196.66 | 195.78 |
| Δ Nb—O | Nb1 (pm) | 30.1 | 28.3 | 33.4 | 16.1 |
| Nb—O distance | Nb2 (pm) | 198.16 | 197.83 | 197.19 | 196.57 |
| Δ Nb—O | Nb2 (pm) | 30.2 | 28.2 | 23.9 | 7.7 |

of the respective s.o.f. values. The total relative occupancy for the $A2$ sites is *ca* 90%.

The site-occupancy factors and their compositional dependence can be described by a simple statistical model. Assuming that Ba occupies only $A2$ sites and Sr randomly occupies $A1$ and the remaining $A2$ sites with different preferences yields the respective s.o.f. values as a function of the strontium fraction $x$

$$\text{s.o.f.(Ba}-A2) = \frac{N}{Z}(1-x) = \frac{5}{8}(1-x) \tag{5}$$

$$\text{s.o.f.(Sr}-A1) = \frac{5x}{8+4K(5x-1)} \tag{6}$$

$$\text{s.o.f.(Sr}-A2) = \frac{5}{8}x - \frac{5x}{8+4K(5x-1)}. \tag{7}$$

$K$ is a factor denoting the preference of Sr for the $A2$ site compared with $A1$, with $K = 1$ for equal preferences. The results of the model calculation for $K = 1.1$, *i.e.* a slight preference for $A2$, are sketched as gray lines in Fig. 5. A satisfactory agreement with the experimental data was found.

### 3.4. Nb—O bond lengths

The Nb—O bond lengths for all the compositions studied lie between 180 and 214 pm. The mean bond length which characterizes the $NbO_6$ octahedron size decreases monotonically with increasing Sr concentration and reaches 195.8 pm for the $x$(Sr) = 0.82, which is only slightly larger than the value of 195.2 pm calculated for the 'ideal' oxygen (ion radius 138 pm) octahedron. The maximal difference between Nb—O bond lengths describes the asymmetry of the Nb position within the octahedron and also becomes smaller for the Sr-richer crystals. The measured unit-cell parameters, site-occupancy factors and Nb—O distances are shown in Table 1. All experimental data are given in Table 2.[1]

[1] Supplementary data for this paper are available from the IUCr electronic archives (Reference: WS5047). Services for accessing these data are described at the back of the journal.

### 3.5. Temperature dependence of the unit-cell parameters

Usually the unit-cell parameters of crystals increase monotonically with increasing temperature owing to the amplitudes of the ionic oscillations, increasing with increasing temperature. Thermal expansion measurements of SBN with $x = 0.5$ (Shorrocks *et al.*, 1982) and $x = 0.6$ (Bhalla *et al.*, 1987), however, show a negative temperature coefficient for the unit-cell parameter $c$ at low temperatures and a positive one at higher temperatures with a minimum value of $c$ near the phase-transition temperature. In contrast to this, the unit-cell parameter $a$ always strictly increases with increasing temperature. Dilatometric measurements, however, are problematic in ferroelectric crystals owing to domain effects. Recent X-ray measurements (Qadri *et al.*, 2005) for SBN with $x = 0.75$ confirm this anisotropic behavior – with a negative temperature coefficient for $c$, a positive one for $a$ – throughout the temperature range investigated. To clarify the behavior, we extended the measurements of Quadri *et al.* (2005) up to higher temperatures on SBN with $x = 0.822$. The results are plotted in Fig. 6.

Our measurements show that X-ray measurements exhibit a similar behavior as found by thermal expansion measurements for other compositions: the $a$ parameter strictly increases with temperature, whereas $c$ decreases at low temperatures and increases at higher ones. An analog behavior has just been shown by neutron scattering measurements (Schefer *et al.*, 2006).

The explanation for this behavior had already been given by Cross *et al.* (1980) and Shrout *et al.* (1981*a*,*b*), who derived an

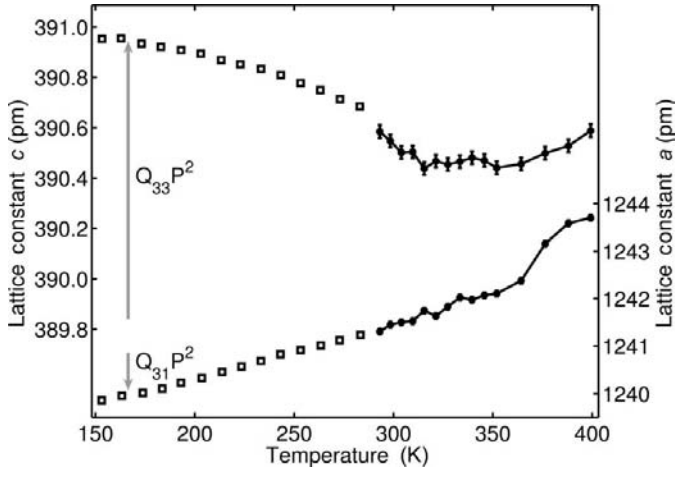


**Figure 6**
Temperature dependence of the unit-cell parameters $a$ and $c$ of SBN with an Sr content of 0.822 (black dots with error bars). For lower temperatures, the results taken from Quadri *et al.* (2005) were plotted (squares) and converted to different compositions (0.75 *versus* 0.822). The gray arrows denote the piezoelectric contributions to the thermal expansion (see text).

**Table 2**
Experimental details.

| | k2shape | sr477 | shape137 | sbn159k3 |
|---|---|---|---|---|
| Crystal data | | | | |
| Chemical formula | $Ba_{0.67}Nb_2O_6Sr_{0.33}$ | $Ba_{0.52}Nb_2O_6Sr_{0.48}$ | $Ba_{0.39}Nb_2O_6Sr_{0.61}$ | $Ba_{0.14}Nb_2O_6Sr_{0.86}$ |
| $M_r$ | 402.26 | 395.44 | 388.68 | 378.29 |
| Cell setting, space group | Tetragonal, *P4bm* | Tetragonal, *P4bm* | Tetragonal, *P4bm* | Tetragonal, *P4bm* |
| Temperature (K) | 298 (2) | 298 (2) | 298 (2) | 298 (2) |
| $a$, $c$ (Å) | 12.4840 (4), 3.9742 (3) | 12.4844 (5), 3.9572 (3) | 12.4575 (7), 3.9382 (3) | 12.4179 (9), 3.9074 (5) |
| $V$ (Å$^3$) | 619.38 (5) | 616.77 (6) | 611.17 (7) | 602.54 (10) |
| $Z$ | 5 | 5 | 5 | 5 |
| $D_x$ (Mg m$^{-3}$) | 5.392 | 5.323 | 5.282 | 5.216 |
| Radiation type | Mo $K\alpha$ | Mo $K\alpha$ | Mo $K\alpha$ | Mo $K\alpha$ |
| $\mu$ (mm$^{-1}$) | 13.33 | 13.78 | 14.31 | 15.13 |
| Crystal form, colour | Sphere, colourless | Sphere, colourless | Sphere, colourless | Sphere, colourless |
| Crystal size (mm) | 0.26 × 0.22 × 0.19 | 0.18 × 0.17 × 0.16 | 0.20 × 0.19 × 0.13 | 0.17 × 0.17 × 0.12 |
| Data collection | | | | |
| Diffractometer | Xcalibur CCD | Xcalibur CCD | Xcalibur CCD | Xcalibur CCD |
| Data collection method | $\omega$ and $\varphi$ | $\omega$ and $\varphi$ | $\omega$ and $\varphi$ | $\omega$ and $\varphi$ |
| Absorption correction | Numerical | Numerical | Numerical | Numerical |
| $T_{min}$ | 0.097 | 0.159 | 0.130 | 0.099 |
| $T_{max}$ | 0.177 | 0.221 | 0.267 | 0.169 |
| No. of measured, independent and observed reflections | 11 682, 2077, 1852 | 11 771, 2157, 1635 | 11 458, 2096, 1740 | 11 273, 2153, 1365 |
| Criterion for observed reflections | $I > 2\sigma$(I) | $I > 2\sigma(I)$ | $I > 2\sigma(I)$ | $I > 2\sigma(I)$ |
| $R_{int}$ | 0.034 | 0.038 | 0.039 | 0.060 |
| $\theta_{max}$ (°) | 40.3 | 41.3 | 39.5 | 43.3 |
| Refinement | | | | |
| Refinement on | $F^2$ | $F^2$ | $F^2$ | $F^2$ |
| $R[F^2 > 2\sigma(F^2)]$, $wR(F^2)$, $S$ | 0.027, 0.065, 1.12 | 0.030, 0.055, 1.00 | 0.033, 0.076, 1.14 | 0.045, 0.091, 0.96 |
| No. of reflections | 2077 | 2157 | 2096 | 2153 |
| No. of parameters | 65 | 65 | 65 | 65 |
| Weighting scheme | $w = 1/[\sigma^2(F_o^2) + (0.0303P)^2 + 1.1155P]$, where $P = (F_o^2 + 2F_c^2)/3$ | $w = 1/[\sigma^2(F_o^2) + (0.021P)^2]$, where $P = (F_o^2 + 2F_c^2)/3$ | $w = 1/[\sigma^2(F_o^2) + (0.0334P)^2 + 0.3182P]$, where $P = (F_o^2 + 2F_c^2)/3$ | $w = 1/[\sigma^2(F_o^2) + (0.0383P)^2]$, where $P = (F_o^2 + 2F_c^2)/3$ |
| $(\Delta/\sigma)_{max}$ | 0.009 | 0.005 | 0.001 | 0.010 |
| $\Delta\rho_{max}$, $\Delta\rho_{min}$ (e Å$^{-3}$) | 2.18, −2.79 | 2.12, −2.80 | 2.54, −3.17 | 3.63, −3.54 |
| Extinction method | *SHELXL* | *SHELXL* | *SHELXL* | *SHELXL* |
| Extinction coefficient | 0.0137 (3) | 0.00421 (12) | 0.0108 (3) | 0.0118 (4) |
| Absolute structure | Flack (1983), 807 Friedel pairs | Flack (1983), 877 Friedel pairs | Flack (1983), 866 Friedel pairs | Flack (1983), 891 Friedel pairs |

Computer programs used: CrysAlisCCD Oxford Diffraction, 2002), *SHELXL*97 (Sheldrick, 1997), WinGX (Farrugia, 1999).

additional electrostrictive contribution to the thermal expansion of ferroelectrics from energetic considerations using the Landau–Ginsburg–Devonshire phenomenological theory. These contributions, $Q_{31}P^2$ for the unit-cell parameter $a$ and $Q_{33}P^2$ for the unit-cell parameter $c$, are plotted as gray arrows in Fig. 6. For the calculation, the electrostriction constants $Q_{ik}$ given by Cross *et al.* (1980) and a typical saturation polarization $P = 0.3$ C m$^{-2}$ were used.

## 4. Conclusion

Structural properties of strontium barium niobate crystals, $Sr_xBa_{1-x}Nb_2O_6$, in the whole range of the tetragonal tungsten bronze phase ($x$ = 0.32–0.82) have been comprehensively studied using powder and single-crystal X-ray diffraction. It has been shown that both unit-cell parameters $a$ and $c$ decrease with increasing $x$, *i.e.* with increasing strontium fraction. This effect can be fully attributed to the composition-dependent fraction of strontium and barium cations on the $A1$ and $A2$ sites, which results in a corresponding dependence of the average effective radii of the cations. Both unit-cell parameters are small compared with those of other TTB-type ferroelectrics. This may be one factor responsible for the high spontaneous polarization and the high electrooptic coefficients of the material.

Using the unit-cell parameters, the X-ray densities were calculated which were in excellent agreement with the macroscopic densities measured. Densities decrease with increasing strontium fraction.

From single-crystal X-ray measurements the site-occupancy factors for the $A1$ and A2 sites were derived; they showed a total occupancy of *ca* 70% for the $A1$ sites and *ca* 90% for the $A2$ sites. Absolute values and composition dependence can be consistently described by a simple statistical model.

The Nb—O distances varied only slightly with composition, whereas the off-center displacements of the Nb atoms showed

a pronounced composition dependence owing to the fact that the phase-transition temperature was near room temperature at higher strontium fractions.

Temperature-dependent measurements of the unit-cell parameters for a composition of $x = 0.822$ confirmed earlier results found for SBN with other compositions. The *a* parameter strictly increases with increasing temperature, whereas the *c* parameter shows a more complicated behavior. At low temperatures *c* decreases, at high temperatures it increases with rising temperature, exhibiting a broad minimum in the region of the phase transition temperature. The effect can be well explained by an electrostrictive contribution to the thermal expansion.

This work was supported by the Graduate College 695 'Nonlinearities of Optical Materials' financed by the Deutsche Forschungsgemeinschaft and the Federal State of Niedersachsen.

## References

Bhalla, A. S., Guo, R., Cross, L. E., Burns, G., Dacol, F. H. & Neurgaonkar, R. R. (1987). *Phys. Rev. B*, **36**, 2030–2035.
Chernaya, T. S., Maksimov, B. A., Verin, I. V., Ivleva, L. I. & Simonov, V. I. (1997). *Crystallogr. Rep.* **42**, 375–380.
Chernaya, T. S., Maksimov, B. A., Volk, T. R., Ivleva, L. I. & Simonov, V. I. (2000). *Phys. Solid State*, **42**, 1716–1721.
Cross, L. E., Shrout, T. & Neurgaonkar, R. R. (1980). *Am. Ceram. Soc. Bull.* **59**, 832.
David, C., Granzow, T., Tunyagi, A., Wöhlecke, M., Woike, T., Betzler, K., Ulex, M., Imlau, M. & Pankrath, R. (2004). *Phys. Status Solidi A Appl. Res.* **201**, R49–R52.
Farrugia, L. J. (1999). *WinGX*, Version 1.61. University of Glasgow, Scotland.
Flack, H. D. (1983). *Acta Cryst.* A**39**, 876–881
Jamieson, P. B., Abrahams, S. C. & Bernstein, J. L. (1968). *J. Chem. Phys.* **48**, 5048.
Neurgaonkar, R. R. & Cory, W. K. (1986). *J. Opt. Soc. Am. B*, **3**, 274.
Neurgaonkar, R. R., Oliver, J. R. & Cross, L. E. (1984). *Ferroelectrics*, **56**, 31–36.
Oxford Diffraction (2002). *CrysAlisRED*, Version 1.69. Oxford Diffraction, UK.
Qadri, S. B., Bellotti, J. A., Garzarella, A. & Wu, D. H. (2005). *Appl. Phys. Lett.* **86**, 251914.
Schefer, J., Schaniel, D., Pomjakushin, V., Stuhr, U., Petricek, V., Woike, Th., Wöhlecke, M. & Imlau, M. (2006). *Phys. Rev. B*, **74**, 134103.
Shannon, R. D. & Prewitt, C. T. (1969). *Acta Cryst.* B**25**, 925–946.
Shannon, R. D. & Prewitt, C. T. (1970). *Acta Cryst.* B**26**, 1046–1048.
Sheldrick, G. M. (1997). *SHELXL*97. University of Göttingen, Germany.
Shorrocks, N. M., Whatmore, R. W. & Liu, S. T. (1982). *J. Phys. D Appl. Phys.* **15**, 2469–2481.
Shrout, T. R., Cross, L. E., Moses, P., McKinstry, H. A. & Neurgaonkar, R. R. (1981*a*). *Ferroelectrics*, **38**, 881.
Shrout, T. R., Cross, L. E., Moses, P., McKinstry, H. A. & Neurgaonkar, R. R. (1981*b*). *IEEE Trans. Son. Ultrason.* **28**, 397.
Ulex, M., Pankrath, R. & Betzler, K. (2004). *J. Cryst. Growth*, **271**, 128–133.
Volk, T., Woike, T., Dörfler, U., Pankrath, R., Ivleva, L. & Wöhlecke, M. (1997). *Ferroelectrics*, **203**, 457–470.
Woike, T., Petricek, V., Dusek, M., Hansen, N. K., Fertey, P., Lecomte, C., Arakcheeva, A., Chapuis, G., Imlau, M. & Pankrath, R. (2003). *Acta Cryst.* B**59**, 28.